



Current-induced second harmonic generation in inversion-symmetric Dirac and Weyl semimetalsKazuaki Takasan ^{1,2,*} Takahiro Morimoto,^{3,4} Joseph Orenstein ^{1,2} and Joel E. Moore^{1,2}¹*Department of Physics, University of California, Berkeley, California 94720, USA*²*Materials Science Division, Lawrence Berkeley National Laboratory, Berkeley, California 94720, USA*³*Department of Applied Physics, The University of Tokyo, Hongo, Tokyo 113-8656, Japan*⁴*JST, PRESTO, Kawaguchi, Saitama 332-0012, Japan*

(Received 23 July 2020; accepted 14 September 2021; published 5 October 2021)

Second harmonic generation (SHG) is a fundamental nonlinear optical phenomenon widely used both for experimental probes of materials and for application to optical devices. Even-order nonlinear optical responses including SHG generally require the breaking of inversion symmetry, and thus have been utilized to study noncentrosymmetric materials. Here, we study theoretically the SHG in inversion-symmetric Dirac and Weyl semimetals under a DC current which breaks the inversion symmetry by creating a nonequilibrium steady state. Based on analytic and numerical calculations, we find that Dirac and Weyl semimetals exhibit strong SHG upon application of finite current. Our experimental estimation for a Dirac semimetal Cd_3As_2 and a magnetic Weyl semimetal $\text{Co}_3\text{Sn}_2\text{S}_2$ suggests that the induced susceptibility $\chi^{(2)}$ for practical applied current densities can reach 10^5 pm V^{-1} with mid-IR or far-IR light. This value is 10^2 – 10^4 times larger than those of typical nonlinear optical materials. We also discuss experimental approaches to observe the current-induced SHG and comment on current-induced SHG in other topological semimetals in connection with recent experiments.

DOI: [10.1103/PhysRevB.104.L161202](https://doi.org/10.1103/PhysRevB.104.L161202)

Introduction. Intense light incident on materials induces various nonlinear optical responses (NLORs) reflecting the details of the material properties [1,2]. The study of NLORs remains an important topic in condensed matter studies since NLORs not only give rich information about the symmetry of the materials but also yield useful optical devices. In recent years, a close relationship between the NLORs and the notion of band geometry has been revealed [3–8]. In particular, three-dimensional (3D) topological materials can support novel NLORs [9–17]. Among these, inversion-symmetry-broken topological semimetals (SMs) are attracting keen attention as recent optical measurements of TaAs, which is an inversion-symmetry-broken Weyl semimetal (WSM), reported strong second harmonic generation (SHG) with a signal 100 times larger than a typical value in GaAs [13,16], and other strong nonlinear optical properties as well [18,19]. From the theoretical side, various interesting nonlinear optical phenomena have been proposed [9,12,14], including a quantization of the circular photogalvanic effect that originates from the topological properties of WSMs [14,20].

On the other hand, there are various topological SMs preserving inversion symmetry which are also intensively studied. One example is topological Dirac semimetals (DSMs), such as Cd_3As_2 [21–23] or Na_3Bi [24], where the Dirac point is protected by crystalline symmetry. The other example is inversion-symmetric magnetic WSMs, such as $\text{Co}_3\text{Sn}_2\text{S}_2$ [25] or Mn_3Sn [26], where the time-reversal symmetry is broken instead of the inversion symmetry. In these materials, odd-order NLORs are only allowed, where the dominant

effect is the third-order NLOR [17]. However, once the inversion symmetry is broken by applying a suitable perturbation, inversion-symmetric materials can also exhibit even-order NLORs.

Motivated by this idea and by general interest in the creation of nonequilibrium states with new or amplified responses, we investigate the creation of second-order NLORs in inversion-symmetric Dirac/Weyl SMs. For the inversion-symmetry-breaking perturbation, we consider a DC electric field which makes the electron distribution asymmetric in momentum space and induces finite current, resulting in broken inversion symmetry. In this Letter, we focus on SHG, which is a phenomenon where injected light with frequency ω is converted into light with a doubled frequency 2ω as schematically shown in Fig. 1 [27]. SHG from current-driven materials has been called current-induced SHG (CISHG) and studied theoretically [28–30] and experimentally in several materials, such as Si [31], GaAs [32], graphene [33,34], and superconducting NbN [35].

Still, CISHG in topological materials, especially Dirac/Weyl SMs, has yet to be explored. Here, we study CISHG in Dirac/Weyl SMs by taking two complementary approaches. One is an analytic calculation with ideal Weyl (Dirac) Hamiltonians and the other is numerical, based on tight-binding models. The results of both approaches are consistent and show that inversion-symmetric Dirac/Weyl SMs support a divergently large CISHG when the Fermi level is located near the Dirac/Weyl points. Based on our results, we estimate the order of the nonlinear susceptibility $\chi^{(2)}$, characterizing the strength of the CISHG. We consider the realistic parameters corresponding to the materials, a Dirac SM, Cd_3As_2 , and a Weyl SM, $\text{Co}_3\text{Sn}_2\text{S}_2$, and find

*takasan@berkeley.edu

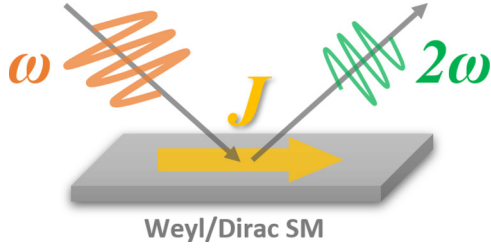


FIG. 1. Concept of current-induced second harmonic generation. Dirac/Weyl semimetals (SMs) in a nonequilibrium state carrying finite current show induced second harmonic generation (SHG), i.e., probe light with frequency ω is converted into outgoing light with frequency 2ω .

that it can reach 10^5 pm V $^{-1}$ for practical applied current densities. These values are 10^2 – 10^4 times larger than those of typical nonlinear materials [13,36,37]. We also address the experimental methods to observe the CISHG and the possibility of CISHG in other topological SMs. Our results suggest that inversion-symmetric topological materials can be a promising material platform to explore NLORs, even those requiring inversion breaking. Because the CISHG in both Dirac and Weyl SMs is large and highly controllable, it can be used in experiments to investigate the nonequilibrium physics of topological materials and future optical devices.

Methods. SHG is characterized by the response tensor $\sigma_{\text{SHG}}^{abc}$ defined via $j^a(2\omega) = \sigma_{\text{SHG}}^{abc}(\omega)E^b(\omega)E^c(\omega)$, where $j^a(2\omega)$ [$E^a(\omega)$] is the Fourier component of the time-dependent current $j^a(t)$ [electric field $E^a(t)$] proportional to $e^{2i\omega t}$ [$e^{i\omega t}$]. The indices a, b, c run over $\{x, y, z\}$ and the sum over repeated indices is implied throughout this Letter. From the standard time-dependent perturbation theory [38–40], we have the following expression for the SHG response tensor,

$$\sigma_{\text{SHG}}^{abc}(\omega) = \sigma_{2p,I}^{abc}(\omega) + \sigma_{2p,II}^{abc}(\omega) + \sigma_{1p,I}^{abc}(\omega) + \sigma_{1p,II}^{abc}(\omega), \quad (1)$$

where

$$\sigma_{2p,I}^{abc}(\omega) = \frac{e^3}{2\hbar^2\omega^2} \int [d\mathbf{k}] v_{mn}^a w_{nm}^{bc} f_{mn} R_\gamma(2\omega - \omega_{nm}), \quad (2)$$

$$\sigma_{2p,II}^{abc}(\omega) = \frac{e^3}{2\hbar^2\omega^2} \int [d\mathbf{k}] \frac{2v_{mn}^a \{v_{np}^b v_{pm}^c\}}{\omega_{np} + \omega_{np}} f_{mn} R_\gamma(2\omega - \omega_{nm}), \quad (3)$$

$$\begin{aligned} \sigma_{1p,I}^{abc}(\omega) &= \frac{e^3}{2\hbar^2\omega^2} \int [d\mathbf{k}] (w_{mn}^{ab} v_{nm}^c + w_{mn}^{ac} v_{nm}^b) \\ &\quad \times f_{mn} R_\gamma(\omega - \omega_{nm}), \end{aligned} \quad (4)$$

$$\begin{aligned} \sigma_{1p,II}^{abc}(\omega) &= \frac{e^3}{2\hbar^2\omega^2} \int [d\mathbf{k}] \frac{v_{mn}^a \{v_{np}^b v_{pm}^c\}}{\omega_{pm} + \omega_{pn}} \\ &\quad \times \{f_{mp} R_\gamma(\omega - \omega_{pm}) - f_{np} R_\gamma(\omega - \omega_{np})\}, \end{aligned} \quad (5)$$

with $v^a = (1/\hbar)\partial_{k_a} H$, $w^{ab} = (1/\hbar)\partial_{k_a}\partial_{k_b} H$, $\{v_{np}^b v_{pm}^c\} = v_{np}^b v_{pm}^c + v_{np}^c v_{pm}^b$, $f_{mn} = f_m - f_n$, $f_n = f(\varepsilon_n)$, $\omega_{mn} = (\varepsilon_m - \varepsilon_n)/\hbar$, and $R_\gamma(x) = 1/(x - i\gamma)$, where the integration $\int [d\mathbf{k}] \equiv \int dk_x dk_y dk_z / (2\pi)^3$ is performed over the entire Brillouin zone [41]. Here, $\varepsilon_n = \varepsilon_n(\mathbf{k})$ represents the n th band of the Hamiltonian $H = H(\mathbf{k})$ (the implicit sum over repeated indices is also taken for the band indices m, n ,

and p) and $f(\varepsilon)$ is a distribution function of electrons. In equilibrium $f(\varepsilon) = f^{(0)}(\varepsilon) \equiv (1 + e^{\beta\varepsilon})^{-1}$, which is the Fermi distribution function with inverse temperature β . The subscript 2p (1p) denotes the contribution of two-photon (one-photon) resonance and the subscript I (II) denotes that the term does (not) contain the factor w^{ab} , which becomes zero in a linearized Hamiltonian.

To calculate the response tensor of CISHG, we need the distribution function of a nonequilibrium steady state (NESS) carrying finite current. To obtain it, we use the Boltzmann equation with the relaxation time approximation under a static electric field \mathbf{E}_{DC} , which is $-(e\mathbf{E}_{\text{DC}}/\hbar)(\partial f_n/\partial \mathbf{k}) = -(f_n - f_n^{(0)})/\tau$, where τ denotes the relaxation time [5,42–44]. Note that we can use this approach only when the interband transition by \mathbf{E}_{DC} is negligible [45]. Solving this equation recursively, we obtain the distribution function for NESS as

$$f_n = f_n^{(0)} + \mathcal{E}_a \frac{\partial f_n^{(0)}}{\partial k_a} + \mathcal{E}_a \mathcal{E}_b \frac{\partial^2 f_n^{(0)}}{\partial k_a \partial k_b} + \dots, \quad (6)$$

with $\mathcal{E}_a = e\tau E_{\text{DC}}^a/\hbar$. We use f_n in Eqs. (2)–(5) to calculate the current-induced SHG. The example of f_n under the electric field in the z direction is shown in the right panel of Fig. 2(b) and the equilibrium distribution $f_n^{(0)}$ is also shown in the left panel of Fig. 2(b) for reference. From these figures, we can see the distribution function is deformed and asymmetric in the k_z direction under the electric field.

Analytic results with Weyl Hamiltonian. To study the CISHG in inversion-symmetric Dirac/Weyl SMs, we take two complementary approaches. One approach is based on a simple Weyl Hamiltonian

$$H_{\text{Weyl}} = \chi v(\mathbf{p} - \mathbf{p}_0) \cdot \boldsymbol{\sigma} - \mu\sigma_0, \quad (7)$$

where $\sigma_{x,y,z}(\sigma_0)$ represents Pauli matrices (2×2 identity matrix), $\boldsymbol{\sigma} = (\sigma^x, \sigma^y, \sigma^z)$, $v = ta/\hbar$ (t and a correspond the hopping amplitude and the lattice constant, respectively), $\mathbf{p} = \hbar\mathbf{k} = \hbar(k_x, k_y, k_z)$, and $\mathbf{p}_0 = \hbar\mathbf{k}_0$. The Hamiltonian H_{Weyl} represents a single Weyl ($\chi = +1$) or anti-Weyl ($\chi = -1$) node located at $\mathbf{k} = \mathbf{k}_0$ [the band structure is shown in Fig. 2(a)]. This Hamiltonian is very simple, but the low-energy physics of Dirac/Weyl SMs are well described by this Hamiltonian [46]. WSMs have pairs of Weyl and anti-Weyl nodes and they locate at different points. On the other hand, DSMs support Weyl and anti-Weyl nodes at the same point, which is called a Dirac node. In the following, we start from a calculation of the SHG of a single (anti-)Weyl node and then sum up the contributions from all the nodes [47]. For simplicity, we assume that the electric fields are applied in the z direction [$\mathbf{E}_{\text{DC}} = (0, 0, E_z)$].

By a straightforward calculation with the Weyl Hamiltonian (7) [48], we can evaluate Eq. (1) analytically at zero temperature. Considering the symmetry, the independent nonzero components are only zzz , zxx , and xzx components [1,2,49]. The zzz component of the response tensor from a single Weyl node is given as

$$\sigma_{\text{single}}^{zzz}(\omega) = \frac{e\tau E_z a \hbar}{\hbar} \frac{e^3}{t \hbar^2} \left\{ -\frac{4}{15} F_{2p}(\omega) + \frac{1}{30} F_{1p}(\omega) \right\}, \quad (8)$$

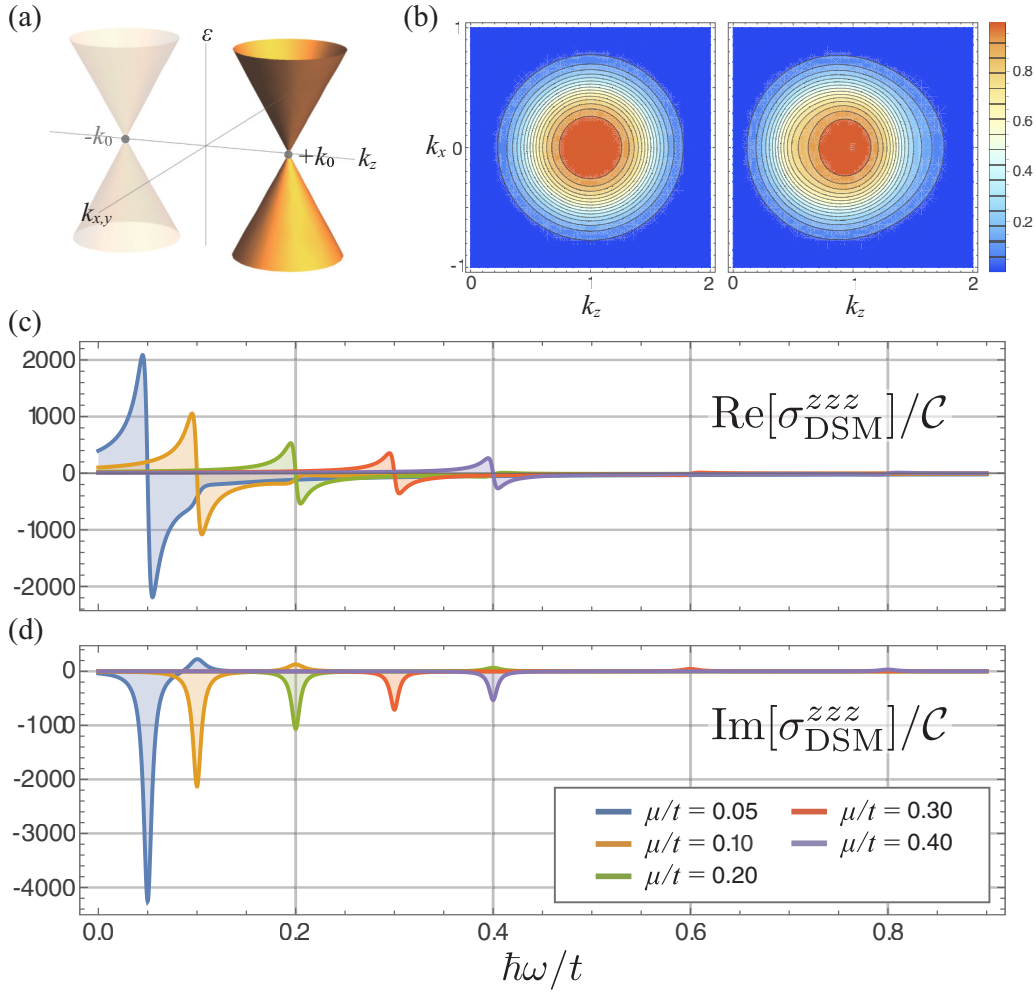


FIG. 2. (a) Energy dispersion of the Weyl Hamiltonian [Eq. (7)] whose gapless point is located at $\pm k_0 = (0, 0, \pm k_0)$. (b) Equilibrium distribution function $f^{(0)}(\varepsilon(\mathbf{k}))$ (left) and nonequilibrium distribution function $f(\varepsilon(\mathbf{k}))$ up to the order of \mathcal{E}_a^2 (right) in momentum space (k_y is fixed to zero). Here, $\varepsilon(\mathbf{k})$ denotes the larger eigenvalue of the Weyl Hamiltonian and the parameters are set as $t = 1$, $a = 1$, $\mu = 0.5$, $k_0 = 1.0$, $\beta = 10$, and $(\mathcal{E}_x, \mathcal{E}_y, \mathcal{E}_z) = (0, 0, 0.1)$. (c), (d) Real and imaginary parts of the CISHG response tensor of Dirac semimetals $\sigma_{\text{DSM}}^{zzz}(\omega)$ calculated with the Weyl Hamiltonian. The values of the vertical axes are normalized by a constant $\mathcal{C} = (\varepsilon t E a / \hbar)(\hbar/t)(e^3/h^2)$. Here, we set $\gamma = 0.01(t/\hbar)$.

with

$$F_{2p}(\omega) = \frac{t}{|\mu|} \frac{t/\hbar}{\omega - |\mu/\hbar| - i\gamma/2}, \quad (9)$$

$$F_{1p}(\omega) = \frac{t}{|\mu|} \frac{t/\hbar}{\omega - 2|\mu/\hbar| - i\gamma}. \quad (10)$$

The other independent components are given as $\sigma_{\text{single}}^{zxz}(\omega) = \mathcal{C}\{-(2/15)F_{2p}(\omega) + (3/10)F_{1p}(\omega)\}$ and $\sigma_{\text{single}}^{xzx}(\omega) = \mathcal{C}\{(1/5)F_{2p}(\omega) - (7/60)F_{1p}(\omega)\}$ with $\mathcal{C} = (\varepsilon t E_a a / \hbar)(\hbar/t)(e^3/h^2)$ [48]. The differences between the components are only numerical factors and their qualitative behaviors are same. Thus, we focus on the zzz component below.

Using these results, we can obtain the CISHG response tensor for Dirac/Weyl SMs. Since the above results do not depend on the position and the chirality of the Weyl nodes, we can calculate the response tensor simply by multiplying the number of Weyl nodes considering the degeneracy. Therefore, assuming that Weyl (Dirac) SMs have two Weyl

(Dirac) nodes [50], the response tensors for Weyl and Dirac SMs are $\sigma_{\text{WSM}}^{zzz}(\omega) = 2\sigma_{\text{single}}^{zzz}(\omega)$ and $\sigma_{\text{DSM}}^{zzz}(\omega) = 4\sigma_{\text{single}}^{zzz}(\omega)$, respectively. The real and imaginary parts of $\text{Re}[\sigma_{\text{DSM}}^{zzz}(\omega)]$ are shown in Figs. 2(c) and 2(d). From these figures and Eqs. (8)–(10), we can see that the SHG spectra have a large peak around $\hbar\omega = \mu$ (two-photon resonance) and a small peak around $\hbar\omega = 2\mu$ (one-photon resonance). The height of the two peaks is proportional to $1/\mu$ [51], leading to a diverging enhancement with $\mu \rightarrow 0$ [52]. This suggests that Dirac/Weyl SMs where the Fermi level is near the Dirac/Weyl points can show strong SHG [45]. The divergent behavior comes from the gapless nodes which are protected by the band topology [18,53].

Numerical results with tight-binding models. Let us move on to the numerical calculation with a tight-binding Hamiltonian describing DSMs. This approach is closer to real materials than the previous approach because we consider multiple (in this model, four) bands and take the nonlinearity and periodicity of the band structure into account. We use the

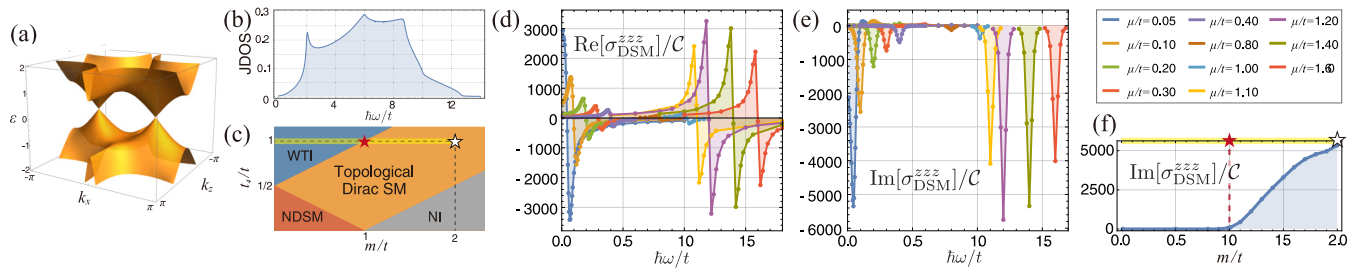


FIG. 3. (a) Energy dispersion, (b) joint density of states (JDOS), and (c) topological phase diagram of the tight-binding model [Eq. (11)]. NDSM, WTI, and NI denote normal (i.e., topologically trivial) Dirac semimetal, weak topological insulator, and normal insulator, respectively. The white star symbol corresponds to the value for (d) and (e). (d), (e) Real and imaginary parts of the CISHG response tensor of Dirac semimetals $\sigma_{\text{DSM}}^{\text{zzz}}(\omega)$ calculated with the tight-binding Hamiltonian. The values in the vertical axes are normalized by a constant $C = (e\tau E_z a/\hbar)(\hbar/t)(e^3/h^2)$. The parameters that we used are $t = 1.0$, $t_1 = 1.0$, $t_2 = 2.0$, $t_3 = 1.0$, $t_4 = 1.0$, $m = 2.0$, $\beta = 100$, and $\gamma = 0.01(t/\hbar)$. (f) m dependence of the peak value in $\sigma_{\text{DSM}}^{\text{zzz}}/C$ at $\hbar\omega = \mu = 0.05t$. Other parameters are the same as those in (d) and (e). The red star symbol corresponds to the topological phase transition.

following tight-binding model,

$$H_{\text{TB}}(\mathbf{k}) = f_1(\mathbf{k})\sigma_z\tau_x + f_2(\mathbf{k})\sigma_0\tau_y + f_3(\mathbf{k})\sigma_x\tau_x + f_4(\mathbf{k})\sigma_y\tau_x + f_5(\mathbf{k})\sigma_0\tau_3, \quad (11)$$

with

$$f_1(\mathbf{k}) = t_1 \sin(ak_x), \quad f_2(\mathbf{k}) = -t_1 \sin(ak_y), \quad (12)$$

$$f_3(\mathbf{k}) = (t_2 + t_3)[\cos(ak_y) - \cos(ak_x)] \sin(ak_z), \quad (13)$$

$$f_4(\mathbf{k}) = -(t_2 - t_3) \sin(ak_x) \sin(ak_y) \sin(ak_z), \quad (14)$$

$$f_5(\mathbf{k}) = m - t_4\{\cos(ak_x) + \cos(ak_y)\} - t \cos(ak_z), \quad (15)$$

introduced in Ref. [53]. As shown in the topological phase diagram [Fig. 3(c)], this model hosts several topological phases. In particular, the topological DSM phase is realized in a wide range of parameters. In this phase, the energy dispersion has a pair of Dirac points located on the k_z axis [Fig. 3(a)]. These Dirac cones are protected by the C_4 rotational symmetry and topologically robust, which is also the case in the typical topological DSM material, Cd_3As_2 [53].

Using this model, we calculate the SHG response tensor $\sigma_{\text{DSM}}^{\text{zzz}}(\omega)$ under the z -directed electric field $\mathbf{E}_{\text{DC}} = (0, 0, E_z)$ at finite temperature [54]. By numerical calculations, we obtain the SHG spectra shown in Figs. 3(d) and 3(e). First, we find strong peaks around $\hbar\omega \sim \mu$ for $\mu \sim 0$ and they show a divergent enhancement as $\mu \rightarrow 0$. These are consistent with our analytic results. Thus, we conclude this behavior comes from the topologically protected Dirac nodes. Indeed, changing the parameter from the Dirac SMs to the other gapped regime, the response vanishes at the topological phase transition point as shown in Fig. 3(f). Note that the same behavior also appears in the other nonzero components zxx and xzx [48]. The other important feature in the spectra is the appearance of a large peak when $\mu/t \sim 1.1$ – 1.6 . This behavior reflects the van Hove singularity at $\mu/t = 1.0$. Indeed, the joint density of states (JDOS) [55] shows a singularity at $\hbar\omega/t \sim 2.0$ as shown in Fig. 3(b) [56]. Note that this peak is very small in the other components because the band structure around the van Hove singularity is strongly anisotropic [48]. We also study the tight-binding model for the Weyl SMs [57]. The results are also consistent with our analytical results and show a similar divergent response as $\mu \rightarrow 0$ [48].

Discussion. Our calculation suggests that Dirac and Weyl SMs show very strong CISHG. To connect these results with experiments, we estimate the strength of CISHG. First of all, we need to specify an experimental setup to give an estimate because the achievable electric field depends on the type of experiment. We propose two kinds of experimental setups shown in Fig. 4 [58]. One is a standard SHG measurement under a DC bias voltage. The other is a THz pump SHG measurement, where the pump frequency is low enough to be seen as a static field [59]. The former approach is static and thus should be easier than the other one, which is time resolved. On the other hand, the latter approach is advantageous for applying a strong electric field because very strong THz fields such as 1–80 MV/cm has been achieved [60].

Next, we estimate the strength of the electric fields inside the material. For the DC bias case, the experimental control parameter is current density rather than field strength. Following the Ohm's law, the internal electric field E_{in} is given as $E_{\text{in}} = j/\sigma$, where j and σ are the current density and the conductivity, respectively. For the THz pump case, we have to take into account the mismatch of impedance. The internal electric field is represented as $E_{\text{in}} = 2E_{\text{ext}}/(n+1)$ with the external pump field E_{ext} and the refractive index n . In the

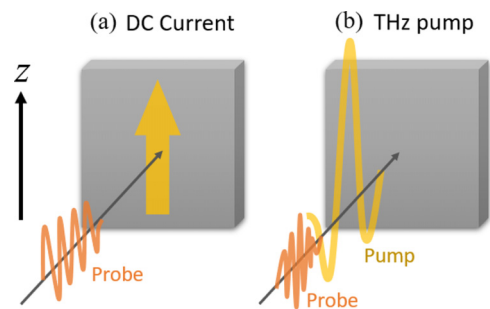


FIG. 4. Two experimental approaches to observation of CISHG. (a) Standard SHG measurement with applying a DC bias voltage to induce a current. (b) Pump-probe-type SHG measurement. The pump pulse should be at low enough frequency compared to interband excitations that the induced state is the same as that created by a DC voltage, which for most materials extends up to the terahertz (THz) range.

THz regime, the refractive index is given as $n = \sqrt{\sigma/(i\Omega\epsilon_0)}$, where ϵ_0 is the vacuum permittivity and Ω is the pump field frequency. To be specific, we consider two materials: a Dirac semimetal, Cd_3As_2 , and a Weyl semimetal, $\text{Co}_3\text{Sn}_2\text{S}_2$ [61]. Using the low temperature conductivity of these materials [62] and assuming $j \sim 10^7$ A/m², $E_{\text{ext}} \sim 400$ kV/m, and $\Omega \sim 0.5$ THz as typical values, we obtain $E_{\text{in}} \sim 4.4$ (30) V/m for the DC bias case and $E_{\text{in}} \sim 2$ (4) kV/m for the THz pump case in Cd_3As_2 ($\text{Co}_3\text{Sn}_2\text{S}_2$).

To estimate the strength of CISHG, we evaluate the nonlinear susceptibility $\chi^{zzz} = \sigma^{zzz}/(2i\omega\epsilon_0)$. The susceptibility takes the largest value when the probe frequency is resonant to the Fermi energy, i.e., $\omega \sim \mu/\hbar$, and we consider this resonant case below. The Fermi energy of Cd_3As_2 ($\text{Co}_3\text{Sn}_2\text{S}_2$) is typically 100 (50) meV [23,25,63] and thus the frequency of probe light is 24 (12) THz, which corresponds to the wavelength 12.5 (25) μm in the mid-IR (far-IR) regime. Using the formula (8) with the parameters for Cd_3As_2 ($\text{Co}_3\text{Sn}_2\text{S}_2$) [64], we obtain $|\text{Re } \chi^{zzz}| \sim 1.2 \times 10^3$ (1.1×10^2) pm V⁻¹ in the DC bias case and $|\text{Re } \chi^{zzz}| \sim 5.5 \times 10^5$ (1.1×10^5) pm V⁻¹ in the THz pump case. Compared to the typical value of the susceptibility of SHG, such as 3.6×10^3 pm V⁻¹ of TaAs (the fundamental wavelength $\lambda = 800$ nm) [13], 3.5×10^2 pm V⁻¹ of GaAs ($\lambda = 810$ nm) [36], 15–19 pm V⁻¹ of BiFeO₃ ($\lambda = 1.55$ μm) [37], the values evaluated above are very large and suggest that Cd_3As_2 and $\text{Co}_3\text{Sn}_2\text{S}_2$ are promising candidates showing very strong CISHG. For the DC bias case, the response is relatively small because the internal electric fields are small, but CISHG of Cd_3As_2 can be comparable to SHG of TaAs due to its longer relaxation time. Remarkably, the responses of both Cd_3As_2 and $\text{Co}_3\text{Sn}_2\text{S}_2$ in the THz pump case are 10^2 times larger than that of TaAs, which has the largest $\chi^{(2)}$, and 10^4 times larger than that of BiFeO₃ [65].

We comment on the possibility of the CISHG in other topological SMs. Since our analytic results are only based on the simple Weyl point Hamiltonian without any assumption about symmetry, similar CISHGs can occur even in inversion-symmetry-broken Weyl SMs, such as TaAs. Such materials are expected to show a large CISHG in addition to the original

SHG, and these two contributions are separable via changing the applied electric field. Very recent experiments [66] suggest that indeed the CISHG component is detectable in TaAs using an optically pumped current, which is found to change the symmetry of SHG in the plane perpendicular to that material's polar axis; our model predicts that the signal induced in Cd_3As_2 should be much stronger because its relaxation time is at least an order of magnitude longer. Furthermore, our tight-binding calculation suggests that the van Hove singularities can be an origin of a large CISHG while they are not divergent as the CISHG from Weyl nodes. Thus, since topological nodal SMs have van Hove singularities protected by its topology, they are also expected to be candidate materials showing strong CISHG.

In this Letter, we have shown that Dirac/Weyl SMs with inversion symmetry show very strong CISHG, and inversion-breaking topological SMs may also be expected to show strong CISHG on top of the zero-current ordinary SHG. These results suggest that topological SMs have value as a nonlinear optical material whose SHG intensity is controllable from zero to a very large value by electric current. Moreover, the SHG is also controlled by changing the direction of the current. This high degree of control can provide another route to realize switchable nonlinear optical devices.

Acknowledgments. We thank Daniel E. Parker for valuable discussions. This work was primarily supported by the U.S. Department of Energy, Office of Science, Office of Basic Energy Sciences, Materials Sciences and Engineering Division under Contract No. DE-AC02-05-CH11231 within the Quantum Materials program (KC2202) (J.W.O. and J.E.M.). K.T. thanks JSPS for support from Overseas Research Fellowship. K.T. was partly supported during the period of manuscript preparation by the U.S. Department of Energy (DOE), Office of Science, Basic Energy Sciences (BES), Materials Sciences and Engineering Division under Contract No. AC02-05CH11231 within the Ultrafast Materials Science Program (KC2203). T.M. was supported by JST PRESTO (JPMJPR19L9) and JST CREST (JPMJCR19T3). J.E.M. acknowledges support through a Simons Investigatorship.

-
- [1] N. Bloembergen, *Nonlinear Optics*, 4th ed. (World Scientific, Singapore, 1996).
 - [2] R. W. Boyd, *Nonlinear Optics*, 3rd ed. (Academic, London, 2008).
 - [3] J. E. Moore and J. Orenstein, *Phys. Rev. Lett.* **105**, 026805 (2010).
 - [4] E. Deyo, L. E. Golub, E. L. Ivchenko, and B. Spivak, [arXiv:0904.1917](https://arxiv.org/abs/0904.1917).
 - [5] I. Sodemann and L. Fu, *Phys. Rev. Lett.* **115**, 216806 (2015).
 - [6] J. E. Sipe and A. I. Shkrebti, *Phys. Rev. B* **61**, 5337 (2000).
 - [7] S. M. Young and A. M. Rappe, *Phys. Rev. Lett.* **109**, 116601 (2012).
 - [8] T. Morimoto and N. Nagaosa, *Sci. Adv.* **2**, e1501524 (2016).
 - [9] P. Hosur, *Phys. Rev. B* **83**, 035309 (2011).
 - [10] H. Ishizuka, T. Hayata, M. Ueda, and N. Nagaosa, *Phys. Rev. Lett.* **117**, 216601 (2016).
 - [11] A. Cortijo, *Phys. Rev. B* **94**, 235123 (2016).
 - [12] C.-K. Chan, N. H. Lindner, G. Refael, and P. A. Lee, *Phys. Rev. B* **95**, 041104(R) (2017).
 - [13] L. Wu, S. Patankar, T. Morimoto, N. L. Nair, E. Thewalt, A. Little, J. G. Analytis, J. E. Moore, and J. Orenstein, *Nat. Phys.* **13**, 350 (2017).
 - [14] F. de Juan, A. G. Grushin, T. Morimoto, and J. E. Moore, *Nat. Commun.* **8**, 15995 (2017).
 - [15] L. E. Golub and E. L. Ivchenko, *Phys. Rev. B* **98**, 075305 (2018).
 - [16] S. Patankar, L. Wu, B. Lu, M. Rai, J. D. Tran, T. Morimoto, D. E. Parker, A. G. Grushin, N. L. Nair, J. G. Analytis, J. E. Moore, J. Orenstein, and D. H. Torchinsky, *Phys. Rev. B* **98**, 165113 (2018).
 - [17] B. Cheng, N. Kanda, T. N. Ikeda, T. Matsuda, P. Xia, T. Schumann, S. Stemmer, J. Itatani, N. P. Armitage,

- and R. Matsunaga, *Phys. Rev. Lett.* **124**, 117402 (2020).
- [18] G. B. Osterhoudt, L. K. Diebel, M. J. Gray, X. Yang, J. Stanco, X. Huang, B. Shen, N. Ni, P. J. W. Moll, Y. Ran, and K. S. Burch, *Nat. Mater.* **18**, 471 (2019).
- [19] N. Sirica, R. I. Tobey, L. X. Zhao, G. F. Chen, B. Xu, R. Yang, B. Shen, D. A. Yarotski, P. Bownan, S. A. Trugman, J.-X. Zhu, Y. M. Dai, A. K. Azad, N. Ni, X. G. Qiu, A. J. Taylor, and R. P. Prasankumar, *Phys. Rev. Lett.* **122**, 197401 (2019).
- [20] F. Flicker, F. de Juan, B. Bradlyn, T. Morimoto, M. G. Vergniori, and A. G. Grushin, *Phys. Rev. B* **98**, 155145 (2018).
- [21] A. J. Rosenberg and T. C. Harman, *J. Appl. Phys.* **30**, 1621 (1959).
- [22] Z. Wang, H. Weng, Q. Wu, X. Dai, and Z. Fang, *Phys. Rev. B* **88**, 125427 (2013).
- [23] I. Crassee, R. Sankar, W.-L. Lee, A. Akrap, and M. Orlita, *Phys. Rev. Materials* **2**, 120302 (2018).
- [24] Z. Wang, Y. Sun, X.-Q. Chen, C. Franchini, G. Xu, H. Weng, X. Dai, and Z. Fang, *Phys. Rev. B* **85**, 195320 (2012).
- [25] D. F. Liu, A. J. Liang, E. K. Liu, Q. N. Xu, Y. W. Li, C. Chen, D. Pei, W. J. Shi, S. K. Mo, P. Dudin, T. Kim, C. Cacho, G. Li, Y. Sun, L. X. Yang, Z. K. Liu, S. S. P. Parkin, C. Felser, and Y. L. Chen, *Science* **365**, 1282 (2019).
- [26] K. Kuroda, T. Tomita, M.-T. Suzuki, C. Bareille, A. A. Nugroho, P. Goswami, M. Ochi, M. Ikhlas, M. Nakayama, S. Akebi, R. Noguchi, R. Ishii, N. Inami, K. Ono, H. Kumigashira, A. Varykhalov, T. Muro, T. Koretsune, R. Arita, S. Shin, T. Kondo, and S. Nakatsuji, *Nat. Mat.* **16**, 1090 (2017).
- [27] This device geometry is similar to what is used to measure photoconductivity in inversion-symmetric insulators, where an applied DC electric field leads to a current pulse under illumination. In metals, this DC field will already produce some current, so the most visible optical consequence of the field-induced symmetry breaking is now CISHG.
- [28] J. B. Khurgin, *Appl. Phys. Lett.* **67**, 1113 (1995).
- [29] S. Wu, L. Mao, A. M. Jones, W. Yao, C. Zhang, and X. Xu, *Nano Lett.* **12**, 2032 (2012).
- [30] J. L. Cheng, N. Vermeulen, and J. E. Sipe, *Opt. Express* **22**, 15868 (2014).
- [31] O. A. Aktsipetrov, V. O. Bessonov, A. A. Fedyanin, and V. O. Val'dner, *JETP Lett.* **89**, 58 (2009).
- [32] B. A. Ruzicka, L. K. Werake, G. Xu, J. B. Khurgin, E. Y. Sherman, J. Z. Wu, and H. Zhao, *Phys. Rev. Lett.* **108**, 077403 (2012).
- [33] A. Y. Bykov, T. V. Murzina, M. G. Rybin, and E. D. Obraztsova, *Phys. Rev. B* **85**, 121413(R) (2012).
- [34] Y. Q. An, F. Nelson, J. U. Lee, and A. C. Diebold, *Nano Lett.* **13**, 2104 (2013).
- [35] S. Nakamura, K. Katsumi, H. Terai, and R. Shimano, *Phys. Rev. Lett.* **125**, 097004 (2020).
- [36] S. Bergfeld and W. Daum, *Phys. Rev. Lett.* **90**, 036801 (2003).
- [37] R. C. Haislmaier, N. J. Podraza, S. Denev, A. Melville, D. G. Schlom, and V. Gopalan, *Appl. Phys. Lett.* **103**, 031906 (2013).
- [38] D. J. Moss, E. Ghahramani, J. E. Sipe, and H. M. van Driel, *Phys. Rev. B* **41**, 1542 (1990).
- [39] E. Ghahramani, D. J. Moss, and J. E. Sipe, *Phys. Rev. B* **43**, 8990 (1991).
- [40] X. Yang, K. Burch, and Y. Ran, [arXiv:1712.09363](https://arxiv.org/abs/1712.09363).
- [41] These formulas are based on the velocity gauge [38–40]. In contrast, there is another gauge choice known as the length gauge [6,67] and it is known that they give different results in some cases, while this mismatch is resolved taking into account the sum rule [67,68]. We have compared our formulas to ones in the length gauge in Ref. [6] and checked the most dominant contribution $\sigma_{2p,1l}^{zzz}$ is reproduced even in the length gauge. This is natural in that the CISHG originates from the group velocity of optically excited electrons (under an asymmetric electron distribution induced by a DC electric field) and this contribution is incorporated in both descriptions.
- [42] H. Yu, Y. Wu, G.-B. Liu, X. Xu, and W. Yao, *Phys. Rev. Lett.* **113**, 156603 (2014).
- [43] T. Morimoto, S. Zhong, J. Orenstein, and J. E. Moore, *Phys. Rev. B* **94**, 245121 (2016).
- [44] K. Yasuda, A. Tsukazaki, R. Yoshimi, K. S. Takahashi, M. Kawasaki, and Y. Tokura, *Phys. Rev. Lett.* **117**, 127202 (2016).
- [45] Considering the Dirac dispersion, there exists a minimum chemical potential for the application of our theory because the interband transition is not negligible when the chemical potential is sufficiently near the Dirac point and the Boltzmann equation does not work. The minimum value $|\mu_0|$ is estimated from $|\mu_0| \sim \hbar v \Delta k \sim e v \tau E_{DC}$. Using the experimentally estimated values [64], $|\mu_0|$ is 0.01 (0.003) meV under a DC bias voltage and 6.6 (0.33) meV under a THz pump for Cd_3As_2 ($Co_3Sn_2S_2$).
- [46] N. P. Armitage, E. J. Mele, and A. Vishwanath, *Rev. Mod. Phys.* **90**, 015001 (2018).
- [47] There are cases, such as the chiral magnetic effect, in which treating Weyl nodes in isolation of the band structure between them is dangerous. In this case, the issue does not arise as we are perturbing the ground-state occupations only near the Weyl points and the ground-state response is zero by symmetry.
- [48] See Supplemental Material at <http://link.aps.org/supplemental/10.1103/PhysRevB.104.L161202> for the derivation of the response tensor using Weyl Hamiltonian (Sec. S1), the other nonzero components (zxx and xzx) of the response tensor for the tight-binding model (Sec. S2), the explanation about the deviation of the peaks in SHG and JDOS spectra (Sec. S3), and the results of the tight-binding calculation for Weyl semimetals (Sec. S4).
- [49] From the symmetry, $\sigma_{single}^{zxx} = \sigma_{single}^{zyy}$ and $\sigma_{single}^{xzx} = \sigma_{single}^{xxz} = \sigma_{single}^{yzy} = \sigma_{single}^{yyz}$ and the other components are zero.
- [50] A single Dirac node is the simplest assumption, but we consider two Dirac nodes here to compare this result with our tight-binding calculation respecting the features of a Dirac SM material Cd_3As_2 .
- [51] The power of $1/\mu$ is different from that in the graphene case discussed in the previous study [30] because of the different dimensionality. The calculation of the CISHG for a two-dimensional Weyl Hamiltonian corresponding to graphene is given in the Supplemental Material [48], Sec. S1.
- [52] How such small- ω divergences from perturbation theory become regularized has been discussed in undriven systems [8,69], and our work suggests that such models should be extended to nonequilibrium current-induced states. From these previous studies, the divergence $\propto 1/\omega$ is expected to be suppressed in the strong electric field regime due to the induced emission. However, the physical large response should be preserved as reminiscent of the divergence.
- [53] B.-J. Yang and N. Nagaosa, *Nat. Commun.* **5**, 4898 (2014).

- [54] We consider finite temperature only for numerical purposes. The SHG is stronger at lower temperature.
- [55] The JDOS is defined as $\rho(\varepsilon) \equiv 2/(8\pi^3) \int d\mathbf{k} \delta(\varepsilon_c(\mathbf{k}) - \varepsilon_v(\mathbf{k}) - \varepsilon)$, where $\varepsilon_{c(v)}(\mathbf{k})$ denotes the conduction (valence) band dispersion.
- [56] The peak takes the largest value at $\mu/t \sim 1.2$ which slightly deviates from the van Hove singularity point. This is because the group velocity becomes zero at the van Hove point. For the detail of this point, see Supplemental Material [48], Sec. S3.
- [57] S. T. Ramamurthy and T. L. Hughes, *Phys. Rev. B* **92**, 085105 (2015).
- [58] To decrease the propagation effect, we consider the reflection geometry as used for the SHG measurement in a Weyl semimetal TaAs [13].
- [59] To use the THz field, the probe frequency needs to be sufficiently higher than the pump laser so that the pump laser light effectively behaves as a DC field. For instance, when we probe the response around 10 THz, we should use a 0.1–1 THz pump laser.
- [60] J. A. Fülöp, S. Tzortzakis, and T. Kampfrath, *Adv. Opt. Mater.* **8**, 1900681 (2020).
- [61] When the time-reversal symmetry is broken, SHG which comes from other processes can be finite even without current. For example, a response related to both electric and magnetic field $j^a(2\omega) = \sigma_{EB}^{abc} E^b(\omega) B^c(\omega)$ is allowed [70]. Since $\text{Co}_3\text{Sn}_2\text{S}_2$ is ferromagnetic, such a SHG response can appear. In this study, we focus on the SHG written as $j^a(2\omega) = \sigma_{\text{SHG}}^{abc} E^b(\omega) E^c(\omega)$. Note that the CISHG we predict can appear even in time-reversal symmetric material and can be distinguished from its dependence on the current density.
- [62] We use the resistivity $\sigma^{-1} = 4.4 \times 10^{-5}$ (3.0×10^{-4}) Ω cm at 78 (150) K for Cd_3As_2 ($\text{Co}_3\text{Sn}_2\text{S}_2$) taken from Ref. [21] (Ref. [71]).
- [63] Z. K. Liu, J. Jiang, B. Zhou, Z. J. Wang, Y. Zhang, H. M. Weng, D. Prabhakaran, S.-K. Mo, H. Peng, P. Dudin, T. Kim, M. Hoesch, Z. Fang, X. Dai, Z. X. Shen, D. L. Feng, Z. Hussain, and Y. L. Chen, *Nat. Mater.* **13**, 677 (2014).
- [64] From Refs. [21,23,25,63], we take the following parameters for Cd_3As_2 ($\text{Co}_3\text{Sn}_2\text{S}_2$): the lattice constant $a \sim 12.6(3)$ Å, the velocity of the Dirac (Weyl) fermion $v \sim 3.0 \times 10^5$ (7.5×10^4) m/s, and the number of Weyl fermions $N_w \sim 4(6)$. In addition, we estimate the relaxation time τ via the conductivity formula of Dirac fermions $\sigma = (2/3)N_w(e^2/h^3)(\tau E_F^2/v)$ and then obtain $\tau \sim 11(1.1)$ ps. The relaxation time of Cd_3As_2 may look too long, but an ultrafast measurement with a detailed theoretical comparison suggests that the relaxation time is 8 ps in a sample of Cd_3As_2 [17]. These value is consistent with other ultrafast measurements [72–74]. Using this relaxation time, we set $\gamma^{-1} = 10\tau$ conservatively as we are not aware of a direct measurement of quasiparticle linewidth. Also, we use $\mu/t = a\mu/(\hbar v) \sim 0.63$ (0.31) and $\hbar\gamma/t \sim 3.73 \times 10^{-3}$ (3.73×10^{-2}) to evaluate the formula [Eq. (8)].
- [65] It is possible to obtain the large response in the other frequency domains. In the THz regime, the response is expected to be much larger than the mid-IR regime since the CISHG becomes divergently large with $\mu \rightarrow 0$. The analytic result [Eq. (8)] indicates that the resonant response at $\hbar\omega = 1$ –10 meV (i.e., 0.24–2.4 THz) is roughly 10–100 times larger than that at $\hbar\omega = 100$ meV. This enhancement is expected to be realized by changing the doping level. In the higher frequency regime, such as the near-IR or visible regime, the effect of the Dirac cones becomes smaller, while van Hove singularity points due to the merging of the Dirac cones give rise to a large CISHG response. This contribution can be large as shown in Figs. 3(d) and 3(e).
- [66] N. Sirica, P. P. Orth, M. S. Scheurer, Y. M. Dai, M. C. Lee, P. Padmanabhan, L. T. Mix, S. W. Teitelbaum, M. Trigo, L. X. Zhao, G. F. Chen, B. Xu, R. Yang, B. Shen, C. C. Lee, H. Lin, T. A. Cochran, S. A. Trugman, J. X. Zhu, M. Z. Hasan *et al.*, [arXiv:2005.10308](https://arxiv.org/abs/2005.10308).
- [67] C. Aversa and J. E. Sipe, *Phys. Rev. B* **52**, 14636 (1995).
- [68] G. B. Ventura, D. J. Passos, J. M. B. Lopes dos Santos, J. M. Viana Parente Lopes, and N. M. R. Peres, *Phys. Rev. B* **96**, 035431 (2017).
- [69] O. Matsyshyn, F. Piazza, R. Moessner, and I. Sodemann, *Phys. Rev. Lett.* **127**, 126604 (2021).
- [70] M. Fiebig, D. Fröhlich, T. Lottermoser, V. V. Pavlov, R. V. Pisarev, and H.-J. Weber, *Phys. Rev. Lett.* **87**, 137202 (2001).
- [71] K. Fujiwara, J. Ikeda, J. Shiogai, T. Seki, K. Takanashi, and A. Tsukazaki, *Jpn. J. Appl. Phys.* **58**, 050912 (2019).
- [72] C. Zhu, F. Wang, Y. Meng, X. Yuan, F. Xiu, H. Luo, Y. Wang, J. Li, X. Lv, L. He, Y. Xu, J. Liu, C. Zhang, Y. Shi, R. Zhang, and S. Zhu, *Nat. Commun.* **8**, 14111 (2017).
- [73] W. Lu, J. Ling, F. Xiu, and D. Sun, *Phys. Rev. B* **98**, 104310 (2018).
- [74] W. Zhang, Y. Yang, P. Suo, W. Zhao, J. Guo, Q. Lu, X. Lin, Z. Jin, L. Wang, G. Chen, F. Xiu, W. Liu, C. Zhang, and G. Ma, *Appl. Phys. Lett.* **114**, 221102 (2019).